Unedited author manuscript for:
Free energy calculations of pore formation in lipid membranes

N. Awasthi[a] and J. S. Hub[a,b]

[a]Institute for Microbiology and Genetics, Georg-August-Universität Göttingen, Göttingen, Germany; [b]Theoretical Physics, Universität des Saarlandes, Saarbrücken, Germany

ARTICLE HISTORY
Compiled October 11, 2020

ABSTRACT
Aqueous pores over lipid membranes are biologically significant transient structures, and play important roles in membrane permeation, membrane fusion, antimicrobial peptide activity, and controlled transport of drug molecules and ions across cellular boundaries. Over the last 20 years, atomic and coarse-grained simulations have been used extensively to model the formation of transmembrane pores, and have hence provided detailed insight into the structures of open pores and into pathways of pore formation. Various perturbations were imposed *in silico* to derive pore formation, including electric fields, membrane tension, and membrane active peptides. Accurate free-energy calculations of pore formation, which can provide quantitative understanding of transmembrane pores, have remained challenging, in part due to the lack of good reaction coordinates (RCs). In this chapter, we review methods for free energy calculations of pore formation, with a focus on RCs that have been proposed to calculate free energy profiles for pore formation from molecular dynamics simulations.

KEYWORDS
Trans-membrane pores; free energy; reaction coordinate; prepore state; molecular dynamics

1. Introduction

For many biophysical processes such as transport of small molecules and ions, cellular signalling, as well as membrane fusion and fission, the formation of polar defects and trans-membrane pores is a critical and often rate-limiting step (Bennett and Tieleman, 2014; Fuhrmans, Marelli, Smirnova, and Müller, 2015; Jahn, Lang, and Südhof, 2003; LaRocca, Stivison, Mal-Sarkar, Hooven, Hod, Spitalnik, and Ratner, 2015; Lenertz, Gavala, Hill, and Bertics, 2009; Vorobyov, Olson, Kim, Koeppe, Andersen, and Allen, 2014). Formation of pores also provides a mechanism to control cell death, as employed by T cells and natural killer cells to kill virus-infected cells (Kägi, Ledermann, Bürki, Seiler, Odermatt, Olsen, Podack, Zinkernagel, and Hengartner,

CONTACT N. Awasthi. Email: nawasth@gwdg.de; J.S. Hub. Email: jochen.hub@physik.uni-saarland.de

1994; Law, Lukoyanova, Voskoboinik, Caradoc-Davies, Baran, Dunstone, DAngelo, Orlova, Coulibaly, Verschoor, Browne, Ciccone, Kuiper, Bird, Trapani, Saibil, and Whisstock, 2010). Membrane electroporation is an established method for transferring various types of material across membranes, such as RNA and vaccines, with applications in cell biology and medicine (Böckmann, De Groot, Kakorin, Neumann, and Grubmüller, 2008; Neumann, Schaefer-Ridder, Wang, and Hofschneider, 1982). Drugs derived from antimicrobial peptides often act via pore-mediated pathways, and cell-penetrating peptides may deliver cargo across membranes by forming defects in the lipid bilayer (Bechara and Sagan, 2013; Brogden, 2005). The mechanisms underlying antimicrobial and cell-penetrating peptides as well as the formation of fusion pores are far from fully understood. Hence, a quantitative understanding of the process of pore-formation and pore-closure would contribute to a better understanding of transport across cell membranes, and additionally, be beneficial for the design and control of membrane active peptides.

In this chapter, we discuss the free energies for forming pores over lipid bilayers. Such free energies can be calculated from molecular dynamics (MD) simulations where membrane bilayers can be modeled by all-atom or coarse-grained lipid forcefields. We focus on all-atom lipid models since they offer the possibility to model atomic details such as hydrogen bonds, which are likely to play an important role for the energetics of pore formation. For most lipid membranes, pore formation is beyond the scope of equilibrium MD simulations because pores form spontaneously only on long time scales. Hence, enhanced sampling techniques such as the umbrella sampling method are required to induce pores in lipid bilayers (Torrie and Valleau, 1974). In umbrella sampling, a biasing potential is applied along a preselected reaction coordinate (RC), and this potential ensures sampling along the complete RC from one thermodynamic state to another. In our case, this would be a transition from a flat, unperturbed membrane to an open-pore state. Apart from the creation of pores in the simulations, a key motivation of umbrella sampling is that it provides the free-energy profile (or potential of mean force, PMF) along the RC, thereby revealing the free-energy difference between the flat membrane and the open pore, as well as the height of free-energy barrier (if present) along the opening pathway. Since free-energy differences and barriers determine equilibrium probabilities and rates, respectively, obtaining PMFs of pore formation is pivotal for developing a quantitative understanding of pores.

By pulling the membrane along an *ideal* RC, the system would gradually sample the flat-membrane state, the barrier at the transition state (if present), and the open-pore state, and thereby more or less follow the minimum free-energy pathway. However, finding good reaction coordinates for complex transitions is far from trivial. Indeed, problems arise when using non-ideal RCs: (i) the PMF may converge poorly and reveal hysteresis between pore-opening and pore-closing pathways, despite the fact that the PMF, being an ensemble property, should not depend on the direction of the pathway; (ii) barriers along the pore-opening transition may be hidden if the barrier is crossed orthogonal to the RC, i.e. the barrier may be integrated out. Below, we discuss the free energy landscape of membrane pore formation with a special emphasis on the different RCs that have been proposed for calculating PMFs using MD simulations.

2. Membrane pores from experiments

2.1. Stable membrane pores

Experimentally, trans-membrane pores have been investigated in detail using model systems such as vesicles, supported lipid monolayers, or cells. Pores were induced using various stress conditions such as surface tension, temperature, and electrochemical gradients (Akinlaja and Sachs, 1998; Melikov, Frolov, Shcherbakov, Samsonov, Chizmadzhev, and Chernomordik, 2001; Tekle, Astumian, Friauf, and Chock, 2001; Zhelev and Needham, 1993). In the experiments, pores were detected using fluorescence-based techniques such as calcein leakage or using electrophysiology. Transient pores have also been observed in giant unilamellar vesicles under tension (Sakuma and Imai, 2015) Such experiments with model systems have provided estimates for the pore size as well as rates of pore formation and closure.

Membranes pores are also observed in experiments in the presence of membrane active agents such as antimicrobial/cell penetrating peptides or cationic polymers (Brogden, 2005; Zasloff, 2002). Experiments with membrane active agents have led to discussions about the possible structural models for transmembrane pores, such as the carpet model, the toroidal pore model, or the barrel-stave model. There is extensive literature on the topic of membrane pores in the presence of membrane active peptides (Brogden, 2005; Wimley, 2010; Zasloff, 2002).

2.2. Metastable pores proposed from experiments

The lifetime of the pores is an important characteristic. It is mainly determined by the presence and height of a free-energy barrier that must be overcome to close the pore. In the absence of such a barrier, pores will close rapidly and hence reveal short lifetimes. In contrast, in the presence of a barrier, the pores are metastable and may reveal long lifetimes.

Nearly four decades ago, Abidor *et al.* (1979) observed the existence of metastable pores in electrophysiology experiments. The experiments revealed rapid transitions between (i) a poorly conducting but long-living state, sometimes referred to as the "prepore state"; and (ii) a fully-formed, highly-conducting, nanometer-sized aqueous pore. Since the pore may rapidly expand between the narrow prepore and the expanded pore, the conductivity of the pore may fluctuate, underlined by the notion of "flickering pores". To our knowledge, the term "prepore" is not yet clearly defined in the literature. Some authors used the term to characterize intermediate, unstable structures during non-equilibrium simulations of pore formation, such as a thin water needle over the hydrophobic membrane core (Böckmann *et al.*, 2008). Other authors used the term to characterize a metastable, narrow aqueous pore, stabilized by a few tilted lipids (Ting, Awasthi, Müller, and Hub, 2018).

Notably, under membrane tension, long-living large pores with a radius of $\sim 1\mu$m were also observed, stabilized by non-equilibrium solvent flow through the pore (Brochard-Wyart, de Gennes, and Sandre, 2000; Karatekin, Sandre, Guitouni, Borghi, Puech, and Brochard-Wyart, 2003; Moroz and Nelson, 1997; Zhelev and Needham, 1993).

3. Modeling pores in molecular dynamics simulations

In parallel with the experimental observation of membrane pores, MD simulations have been used to study transmembrane pores at molecular detail (Gurtovenko, Anwar, and Vattulainen, 2010; Marrink, Jähnig, and Berendsen, 1996). In MD simulations, pores were formed by applying surface tension(Leontiadou, Mark, and Marrink, 2004; Tieleman, Leontiadou, Mark, and Marrink, 2003), electrostatic membrane potentials (Böckmann *et al.*, 2008; Gurtovenko and Vattulainen, 2005; Tarek, 2005; Tieleman *et al.*, 2003), by simulating membrane-active agents such as antimicrobial or cell-penetrating peptides (Herce, Garcia, Litt, Kane, Martin, Enrique, Rebolledo, and Milesi, 2009; Leontiadou, Mark, and Marrink, 2006; Sengupta, Leontiadou, Mark, and Marrink, 2008), or by inserting small charged solutes into the membrane (Neale, Madill, Rauscher, and Pomès, 2013; Tepper and Voth, 2005). Pores were also observed as metastable intermediate structures during spontaneous aggregation of membranes (Marrink, Lindahl, Edholm, and Mark, 2001). From simulations, disordered toroidal pores have been predicted as structures for transmembrane pores in the presence of membrane active peptides (Leontiadou *et al.*, 2006; Sengupta *et al.*, 2008). MD simulations of pore formation have been reviewed repeatedly, hence we refer to reader to the literature for a more complete view on the field (Bennett and Tieleman, 2014; Kirsch and Böckmann, 2016).

Computationally, metastable pores were reported from simulations of stretched membranes (Tolpekina, Den Otter, and Briels, 2004). In tension-free membranes, however, resolving a pore nucleation barrier in the PMF, as required to rationalize a metastable pore, turned out to be challenging (Awasthi and Hub, 2016; Bennett and Tieleman, 2014; Wohlert, den Otter, Edholm, and Briels, 2006); as shown below, these challenges are primarily associated with problems with RCs. Only recently, using the string method in conjunction with self-consistent field theory or using umbrella sampling calculations with a new RC, a pore nucleation barrier could be resolved (Hub and Awasthi, 2017; Ting *et al.*, 2018).

4. Reaction coordinates for free-energy calculations of pore formation: a comparison

PMF calculations are a standard protocol for obtaining the energetics along functionally relevant transitions in biomolecular systems, such as pore formation in membranes. In principle, it should be possible to compute the free energy landscape for pore formation using MD simulations and enhanced sampling techniques such as umbrella sampling (Torrie and Valleau, 1974). Umbrella sampling requires the definition of one or several suitable reaction coordinates (RCs, or order parameters), along which the system is steered and PMFs are calculated. In the context of pore formation, the RC should steer the system from the state of an intact membrane to the state with an open transmembrane pore. However, identifying good RCs for complex transitions such as pore formation, is often a challenging task (Best and Hummer, 2005; Bolhuis, Chandler, Dellago, and Geissler, 2002; Neale and Pomès, 2016).

Several RCs were implemented for modeling membrane pores, as illustrated in Fig. 1. Pulling the system along these RCs is characterized by

a) steering the lipids radially (or laterally) from the pore center (Tolpekina *et al.*, 2004; Wohlert *et al.*, 2006);
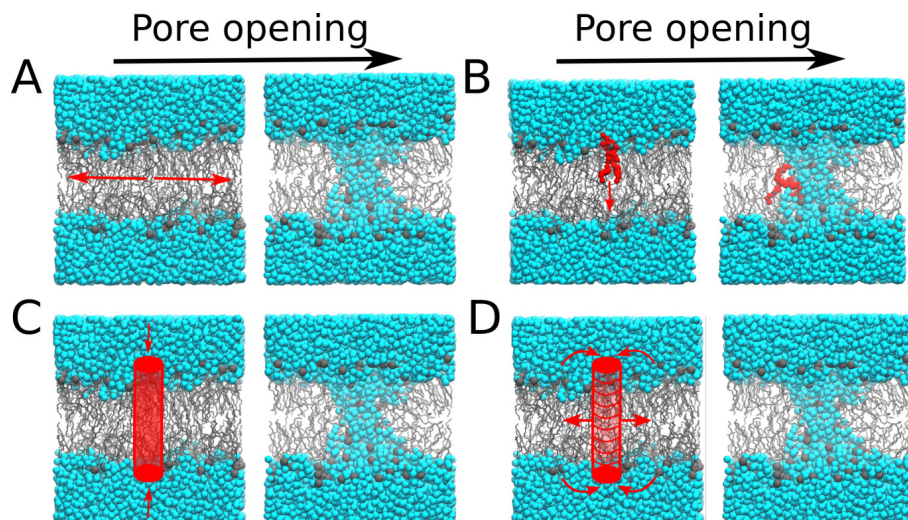
Figure 1. Illustration of four reaction coordinates (RCs) suggested for calculating the potential of mean force of transmembrane pore formation. (A) Collective radial coordinate, (B) the flip-flop coordinate, (C) the average water density in a membrane-spanning cylinder, and (D) the chain coordinate. Lipid molecules are visualized as silver sticks, lipid phosphate atoms as grey spheres, and water molecules as cyan spheres.

  b) pulling a single lipid head group towards the bilayer center, corresponding to a lipid flip-flop transition (Bennett and Tieleman, 2011, 2014; Sapay and Tieleman, 2009; Tieleman and Marrink, 2006);
  c) pulling water into a membrane-spanning cylinder (Mirjalili and Feig, 2015);
  d) generating a hydrogen bond chain over the membrane by filling slices of a membrane-spanning cylinder with polar atoms (Hub and Awasthi, 2017).

Upon pulling the membrane along any of these RCs, pores formed first by the penetration of a thin water needle into the membrane, followed by tilting of lipids parallel to the membrane to avoid unfavorable contacts of water with the apolar membrane interior (Bennett and Tieleman, 2014; Böckmann *et al.*, 2008; Tieleman *et al.*, 2003).

To test the performance of the RCs for pore formation, we focus on three aspects: a) are free energies of pore formation obtained from PMFs along the four coordinates in agreement? b) In case that the open pore is metastable, does the PMF along the RC reveal the barrier between the pore-open and pore-closed states, or is the barrier integrated out? b) Do the computed PMFs along a RC suffer from hysteresis owing to slow convergence, i.e. do the PMFs computed from simulation frames taken from pulling simulations conducted in forward and backward direction not agree? For details about simulation parameters, we refer the reader to the reference list of this chapter.

4.1. Steering lipids laterally from pore center: the collective radial coordinate

The collective radial coordinate ξ_R was proposed by Tolpekina *et al.* (Hu, Sinha, and Patel, 2015; Tolpekina *et al.*, 2004; Wohlert *et al.*, 2006). With this coordinate, a transmembrane pore is created by pushing all lipid molecules radially outwards and parallel to the plane, away from the center of the pore (Fig. 1A). Using a switch function, the RC was designed such that lipids close to the pore are pushed more

strongly than lipids far away from the pore. The RC is

$$\xi_R = \frac{\Sigma - \Sigma_0}{N - \Sigma_0}, \tag{1}$$

$$\Sigma = \sum_{i=1}^{N} \tanh(r_i/\zeta). \tag{2}$$

Here, N is the total number of lipid molecules, and r_i is the lateral distance between the center of the pore and the center of mass of lipid i. According to Eq. 2, Σ increases as the lipids move laterally from the pore center. Here, the hyperbolic tangent $\tanh(\cdot)$ with parameter ζ serves as the switch function that ensures that moving lipids within a distance of $\sim 2\zeta$ from the pore center influences Σ more strongly than moving lipids at larger distances. Consequently, lipids near the pore center also feel a stronger biasing force when the system is pulled along the RC. The parameter ζ also determines the approximate radius of the fully formed pore; a reasonable value was suggested to be $1\,\mathrm{nm}$. The normalization in Eq. 1 is chosen such that that $\xi_R = 0$ denotes the initial state with no pore but a random distribution of lipids, while $\xi_R \approx 1$ corresponds to a fully established trans-membrane pore. Here, Σ_0 is the equilibrium value of Σ, which can be computed prior to a simulation by assuming a random distribution of lipids. This reaction coordinate was originally implemented for constrained MD simulations, and later also applied for umbrella sampling simulations (Awasthi and Hub, 2016).

4.2. Distance of one phosphate group from the membrane center: the flip-flop coordinate

Tieleman, Marrink, and coworkers suggested a RC inspired by lipid flip-flop. The RC is defined as the distance d_{ph} between a single lipid phosphate group and the membrane center (Fig. 1/B) Bennett and Tieleman (2011, 2014); Sapay and Tieleman (2009); Tieleman and Marrink (2006). Using this RC to study pores is mainly motivated from the observation that pulling a phosphate group to the membrane center drags water inside the membrane, thereby triggering the formation of a water pore. Applying this RC for PMF calculations is straightforward since center-of-mass pulling is implemented in many MD suites.

4.3. Average water density inside a membrane-spanning cylinder: water-density coordinate

Whereas the RCs described above steer the lipid molecules to form a pore, Mirjalili and Feig (2015) suggested a coordinate that follows the penetration of water into the membrane (Mirjalili and Feig, 2015). Accordingly, the coordinate is defined as the average water density inside of a membrane-spanning cylinder (Fig. 1/C), with the cylinder axis aligned with the bilayer normal, and placed symmetrically at the membrane center. The RC can be expressed mathematically using an indicator function $f(\mathbf{r})$ for the cylinder, which takes zero outside and unity inside the cylinder. In order to obtain a RC that is differentiable with respect to the atomic coordinates, the function $f(\mathbf{r})$ must be defined with smooth switch functions at the surface of the cylinder. The RC is given by

$$\rho_{\mathrm{cyl}} = \Gamma_V/V, \tag{3}$$

where $V = \int f(\mathbf{r})\mathrm{d}\mathbf{r}$ is the volume of the cylinder, and Γ_V denotes the number of water molecules inside the cylinder. The latter is given by

$$\Gamma_V = \sum_{i=1}^{N_w} f(\mathbf{R}_i) \tag{4}$$

where N_w denotes the total number of water molecules, and $\mathbf{R}_i$ is the Cartesian coordinate of the water oxygen atom i. It is important to note that ρ_{cyl} does not correspond to a three-dimensional density field, but it is instead a scalar quantity that given by the *number* of water molecules inside the cylinder. Below, we normalize ρ_{cyl} with the bulk water density, such that $\rho_{\mathrm{cyl}}/\rho_{\mathrm{bulk}} \approx 1$ corresponds to a fully filled cylinder.

4.4. Generating a continuous polar defect: the chain coordinate

This RC was designed to differentiate between (i) polar defects that partly penetrate in the membrane and (ii) a continuous defect spanning the entire membrane (Hub and Awasthi, 2017). To this end, the RC was defined using a membrane-spanning cylinder that is decomposed into N_s slices along the membrane normal (Fig. 1/D, slice thickness $\sim 1\text{Å}$). Then, the RC is given by the *number* of slices that are occupied by polar heavy atoms. This definition ensures that the RC is modulated purely by adding polar atoms to empty slices, but hardly by adding polar atoms to previously filled slices. Consequently, by pulling the system along the RC towards the open-pore state, the slices are filled one-by-one by polar atoms, thereby forming a continuous hydrogen bond chain over the entire membrane. Hence, we refer to the RC as "chain coordinate" in this work. In turn, by pulling the system back to the closed-pore state, slices are fully depleted from polar atoms, thereby breaking the continuous hydrogen bond chain over the membrane.

The RC was defined as follows:

$$\xi_{\mathrm{chain}} = N_s^{-1} \sum_{s=0}^{N_s-1} \delta_s(N_s^{(p)}) \tag{5}$$

Here, N_s denotes the number of slices, and $N_s^{(p)}$ is the number of polar heavy atoms inside slice s of the membrane-spanning cylinder. The function δ_s is an indicator function that takes zero if no polar atoms are in slice s, and takes a value close to unity if one more polar atoms are in slice s:

$$\delta_s(N_s^{(p)}) \approx \begin{cases} 0 & \text{if } N_s^{(p)} = 0 \\ 1 & \text{if } N_s^{(p)} \geq 1 \end{cases} \tag{6}$$

This property is critical to distinguish between the cases of (i) few slices occupied by many polar atoms, as found in partial defects spanning part of the membrane, and (ii) structures in which every slice is occupied by at least one polar atom, as found in a continuous membrane-spanning polar defect. To ensure that ξ_{chain} is differentiable with respect to the atomic coordinates, δ_s and $N_s^{(p)}$ were formulated using differentiable switch functions (Hub and Awasthi, 2017).

Critically, the x-y position (in the membrane plane) of the membrane-spanning cylinder is not fixed but instead dynamically defined depending on the position of the
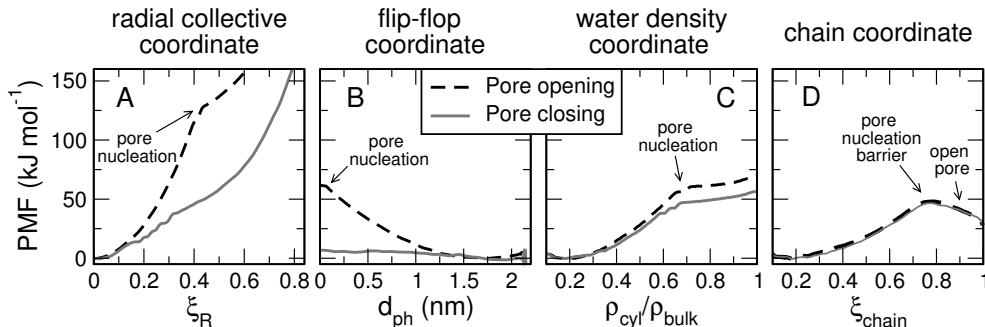
Figure 2. Potentials of mean force (PMF) of transmembrane pore formation in a DMPC membrane, computed along four different reaction coordinates. (A) Collective radial coordinate, (B) flip-flop coordinate, (C) water density, and (D) the chain coordinate. PMFs along pore-opening and pore-closing pathways are shown in black and grey, respectively. For a discussion, see text. Lipids were modeled with the force field by Berger *et al.* (1997), and simulation parameters were chosen as described previously (Awasthi and Hub, 2016).

Table 1. Free energies of a trans-membrane pore and the pore nucleation barrier (if resolved) in a system of 128 DMPC lipids at 300 K modeled with the Berger force field, derived from the PMFs along four reaction coordinates for pore formation.

| Reaction coordinate	Pore free energy[a] (kJ/mol^{-1})	Nucleation barrier (kJ/mol^{-1})	hysteresis
Radial collective, ξ_R (nm)	>125	not resolved	major
Flip-flop, d_{ph} (nm)	60	not resolved	major
Water-density, ρ_{cyl}/ρ_{bulk}	57	not resolved	minor
Chain coordinate, ξ_{chain}	35	48	none

[a]Estimated from PMFs shown in figure 2A-D. In case of hysteresis, the values were taken from the PMFs along the pore-opening pathway.

aqueous defect. In other words, the cylinder follows the defect as the defect explores the membrane plane. This property avoids that the system may move along the RC by shifting the defect laterally out of the cylinder, which was identified as a common source for hysteresis between pore-opening and pore-closing pathways.

4.5. The reaction coordinate greatly influences the PMFs of pore formation

In order to evaluate the performance of the different RCs, we compare the PMFs calculated for a DMPC bilayer with 128 lipid molecules at 300 Kelvin as shown in Figure 2A-D. All PMFs were derived using umbrella sampling windows of 150 ns each, using only the last 50 ns for analysis and omitting the first 100 ns for equilibration. PMFs along pore-opening (black broken lines) and along pore-closing pathways (grey solid lines) are plotted in Fig. 2 A–D as a function of each RCs, i.e. ξ_R, d_{ph}, ρ_{cyl}/ρ_{bulk}, and ξ_{chain}. Evidently, the choice of the RC has a great impact (i) on the estimated free-energy difference between the open pore and the flat membrane, (ii) on undesirable hysteresis between PMFs along pore-opening and pore-closing pathways, and (iii) on the appearance of a nucleation barrier, i.e., whether the open pore is identified as being metastable.

In the following we discuss three important differences between the PMFs shown in Figure 2. Firstly, the free energies of the open pore (relative to the flat membrane) as given by the PMFs differ greatly between the four RCs (Table 1, second column). In particular, the PMF along ξ_R suggests strongly increased free energies as compared to the PMFs along the other three RCs. This indicates that the collective radial
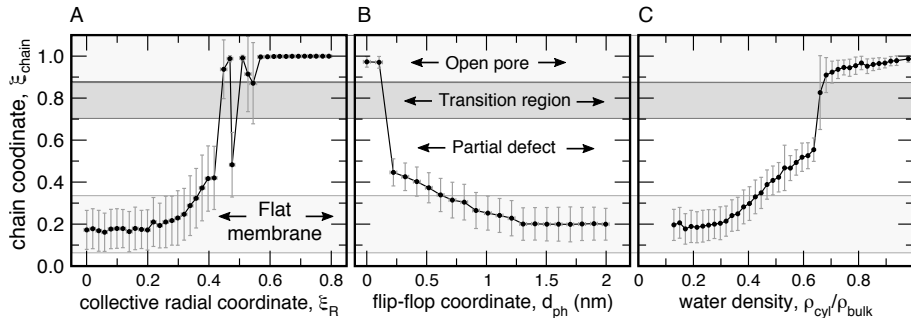
Figure 3. Rationalizing problems with hysteresis and with the lack of a nucleation barrier in a membrane of DMPC: Umbrella sampling simulations restrained along (A) the collective radial collective coordinate ξ_R, (B) the flip-flop coordinate $d_{\rm ph}$, and (C) the water density coordinate $\rho_{\rm cyl}$, projected onto the chain coordinate $\xi_{\rm chain}$. Dots and bars indicate the average and standard deviation of $\xi_{\rm chain}$. The analysis demonstrates that restraining the DMPC membrane along ξ_R, $d_{\rm ph}$, or $\rho_{\rm cyl}$ does not restrain the system close to the transition state of pore formation. Adapted with permission from Hub and Awasthi (2017). Copyright (2017) American Chemical Society.

coordinate perturbs the membrane more strongly than strictly required to form a pore.

Secondly, comparing the PMFs computed along pore-opening and pore closing pathways reveals that the PMFs converge on different time scales. Evidently, the simulations with the radial collective and the flip-flop coordinate strongly suffer from hysteresis. Visual inspection of the trajectories reveals the structural reason for hysteresis. Namely, upon pulling the system along ξ_R or along $d_{\rm ph}$ back towards the flat-membrane state, the aqueous defects simply does not close. In other words, pulling along the ξ_R or $d_{\rm ph}$ RCs is insufficient to break the hydrogen bond network over the membrane, as would be required to close the pore, within 150 ns of simulation. For instance, when pulling the restrained phosphate group from the membrane center ($d_{\rm ph} = 0\,\rm nm$) back to the head group region ($d_{\rm ph} \approx 2\,\rm nm$), the restrained lipid is simply replaced with other lipids, thereby stabilizing the aqueous defect. In contrast, PMFs along the water density coordinate exhibit only minor hysteresis, and the PMFs along the chain coordinate exhibit virtually no hysteresis, suggesting that the PMF are fully converged within 150 ns. This suggests that it is critical to steer the water molecules, and not purely the lipids, in order to break the continuous hydrogen bond network and, hence, to close the pore.

Thirdly, the PMF along the chain coordinate exhibits a barrier for pore nucleation, demonstrating that the open pore forms a metastable state (Fig. 2D). The barrier is compatible with equilibrium simulations on the same system that, starting from an open pore, did not show a pore-closing event within $\sim 10\,\mu\rm s$ of simulation (Awasthi and Hub, 2016). In contrast, PMFs along the other three RCs lack this barrier, suggesting that the barrier was integrated out because the system crosses the barrier in a direction orthogonal to these three RCs (Table 1, third column).

What is the underlying reason for problems with hysteresis and with the loss of the nucleation barrier? This question is addressed in Figure 3, which analyzes umbrella sampling windows restrained along the ξ_R, $d_{\rm ph}$, and $\rho_{\rm cyl}$ coordinates, by projecting each the simulation frames of umbrella window onto the chain coordinate $\xi_{\rm chain}$. The key findings is that, upon pulling the membrane along the radial coordinate, the flip-flop coordinate, or the water density coordinate, the system may sample structures of a flat membrane, of a partial defect, or of the open pore (Fig. 3, horizontal bars); however, the the system hardly samples the transition state of pore formation. In

9
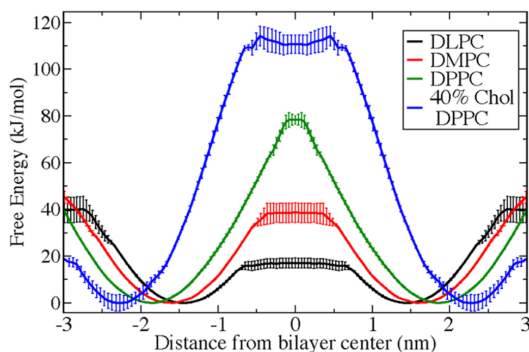
Figure 4. PMFs for pore formation along the flip-flop coordinate for phosphatidylcholine membranes with increasing tail length and as function of cholesterol content. Longer tails and the addition of cholesterol increase the free energy of pore formation. Adapted with permission from Bennett and Tieleman (2014). Copyright (2014) American Chemical Society.

other words, restraining the system along ξ_R, d_{ph}, or ρ_{cyl} does not restrain the system close to the transition state of pore formation. This undesirable property eventually manifests in sampling problems and hysteresis and in the integrated out nucleation barrier.

To conclude, all the reaction coordinates described here have been used successfully to study pore formation in membranes. Simulations employing these coordinates gave atomic-level insight into the structure of pores and the mechanism of pore formation, and they provided the energetics of pore formation at least on a semiquantitative level. However, only the chain coordinate is capable of resolving the nucleation barrier, which is critical for estimating the life time of the pore. In addition, only PMF calculations along the chain coordinate converge rapidly and do not suffer from hysteresis in this system.

5. Longer lipid tails increase the free energy of pore formation

Sapay, Bennett, and Tieleman systematically analyzed the energetics of pore formation in phosphatidylcholine (PC) membranes as function of lipid tail length (Bennett, Sapay, and Tieleman, 2014; Sapay and Tieleman, 2009). Using PMF calculations along the lipid flip-flop coordinate, the authors found that the free energy of pore formation generally increases with the thickness of the membrane (Fig. 4). Later simulations with the chain coordinate confirmed these trends (see also Fig. 5A) (Ting *et al.*, 2018). These findings are rationalized by the fact that pore formation in thicker membranes require the formation of larger aqueous defects before a complete transmembrane pore may form. Further, by decomposing the PMFs into enthalpic and entropic contributions, Bennett *et al.* found that pore formation in PC membranes is opposed by a large loss of entropy, but favored by a gain of enthalpy.

6. Relative volume of lipid head to lipid tails determine the metastability of the pore

Since the pore rim represents a region of high local curvature, it is not surprising that the intrinsic shape of the lipid molecules may influence the energetics of pore
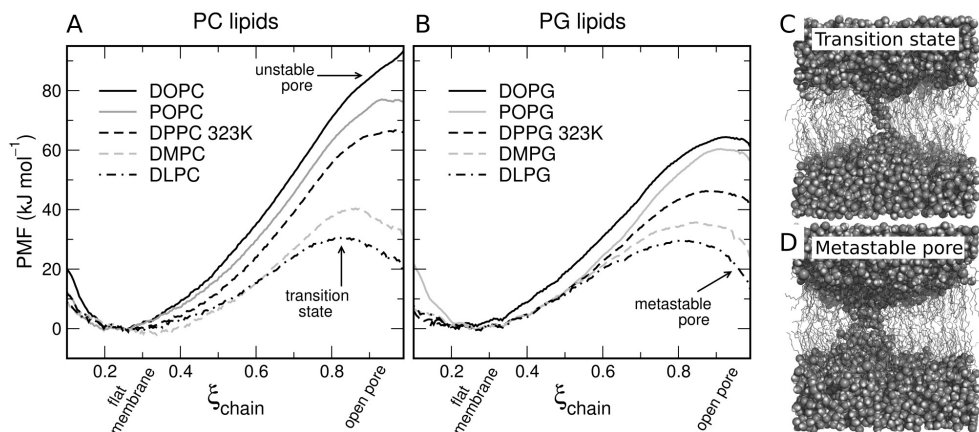
Figure 5. (A/B) PMFs for pore formation calculated using the chain coordinate, ξ_{chain}, for membrane bilayers of different phosphatidylcholine (PC) and phosphoglycerol (PG) lipid molecules with increasing tail length and tail unsaturation. The PMFs were taken from Ting *et al.* (2018), using extended simulation time for DPPC and POPC compared to our previous work. For all PMFs, $\xi_{chain} \sim 0.2$ denotes flat membranes and $\xi_{chain} \sim 1$ denotes open pores. Pronounced nucleation barriers are observed for DLPC, DMPC, DLPG, and DMPG, indicating metastable pores, and shallow barriers for long-tailed PG lipids. For long-tailed PC lipids, no barriers are observed, indicating unstable pores. Lipids were modeled with the Charmm36 force field (Pastor and MacKerell Jr, 2011). PMFs for DPPC and DPPG were computed at 323 Kelvin, all other PMFs at 300 Kelvin. (C) Typical simulation snapshots of a DMPG membrane at the transition state, revealing a thin water needle, and (D) of a fully formed metastable pore. Lipids are shown as sticks, solvent as spheres.

formation. Indeed, Ting *et al.* (2018) showed that lipids with a large head group-to-tail volume ratio form metastable pores, whereas lipids with a small head group-to-tail volume ratio form unstable pores. These findings were obtained by PMF calculations along the chain coordinate with atomistic MD simulations, as well as with a minimal coarse-grained lipid model in conjunction with the string method and self-consistent field theory.

The PMFs along the chain coordinate ξ_{chain} in Fig. 5 demonstrate the effect of the head-to-tail volume ratio on metastability. PMFs are shown for five phosphatidylcholine (PC, Fig. 5A) and five phosphatidylglycerol lipids (PG, Fig. 5B) of increasing tail length and tail unsaturation. Evidently, pores in membranes with short saturated tails such as DLPC, DMPC, DLPG, and DMPG are metastable, demonstrated by the free-energy minimum at $\xi_{chain} \approx 1$ and the nucleation barrier (or transition state) at $\xi_{chain} \approx 0.85$ (Fig.5A/B dot-dashed black, dashed grey curves). This transition state is characterized by a thin water column spanning the complete bilayer, a structure that has been observed in previous studies (Fig. 5C) (Awasthi and Hub, 2016; Bennett and Tieleman, 2014). In PC membranes, lipids with longer tails (DPPC) and longer, unsaturated tails (POPC and DOPC) form unstable pores, as evident from the absence of a nucleation barrier (Fig.5A dashed black, solid grey, and solid black curves). Moreover, owing to the increased volume of PG over PC head groups, shallow nucleation barriers for lipids with longer and unsaturated tails are observed for DPPG, POPG, and DOPG lipids (Fig.5 dashed black, solid grey, and solid black curves respectively). Hence, the increased head-to-tail volume ratio of PG as compared to PC lipids leads correlates with an increased tendency to form metastable pores.

As a simple test of metastability, one can monitor the pore closing times in free simulations starting from an open pore. Figure 6 presents eight unbiased MD simulations of the each of the five PG membranes starting from an open pore. We observe that no pore closed within 200 ns for DLPG and DMPG, confirming the metastability of

11
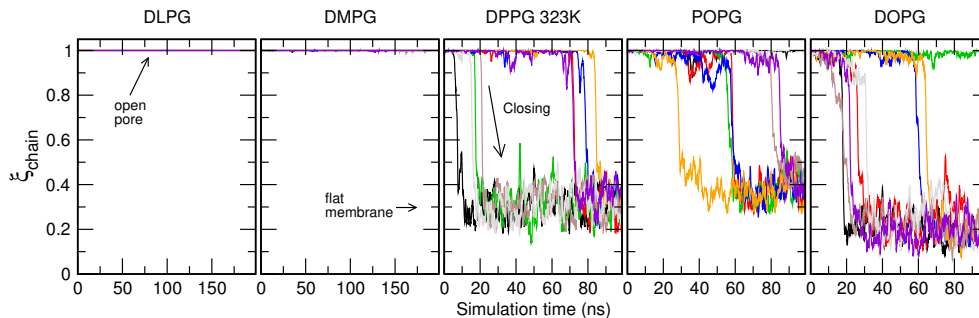
Figure 6. Trajectories of free MD simulations starting from frames with an open pore in phosphatidylglycerol (PG) membranes with increasing tail length and increasing tail unsaturation. Eight independent simulations shown in different colors were conducted for each lipid type (from left to right): DLPG, DMPG, DPPG, POPG, and DOPG. No bias was applied to the simulations. Lipids were modeled with the Charmm36 force field, and simulation parameters were chosen as described previously (Pastor and MacKerell Jr, 2011; Ting *et al.*, 2018). To visualize the spontaneous closing of the pores during the free simulations, the trajectories are projected onto the reaction coordinate ξ_{chain}, where $\xi_{\text{chain}} \approx 1$ and $\xi_{\text{chain}} \approx 0.3$ correspond to open pores and flat unperturbed membranes, respectively (arrows). No pore closed in the bilayers of DLPG and DMPG within 200 ns, confirming the metastability of the pores, and compatible with the pronounced nucleation barriers revealed by the PMF (compare with Fig. 5B). Pores in bilayers of DPPG, POPG, and DOPG closed on the tens of nanosecond time scale, compatible with the shallow nucleation barriers in these membranes.

the pores in DLPG and DMPG, and in line with the pronounced nucleation barriers. In contrast, for DPPG, POPG, and DOPG, the pores close on a time scale of tens of nanoseconds, compatible with the shallower nucleation barrier. These free simulations, corroborated by previous of pore closure simulations in PC membranes (Ting *et al.*, 2018), demonstrate that the PMFs along the chain coordinate indeed reflect the minimum free-energy path of pore formation.

7. Practical consideration for PMF calculations with the chain coordinate

The chain RC requires a number of parameters, which should be chosen correctly to ensure that the PMFs converge rapidly and do not reveal any hysteresis (Hub and Awasthi, 2017). Specifically,

- the thickness of the slices should be chosen such that polar heavy atoms in neighboring slices may form stable hydrogen bonds, even in the presence of some thermal fluctuations. A suitable value is 1 Å;
- the fraction to which a slice is considered as "filled" upon the addition of the first heavy atom. Here, 0.75 was found to be suitable;
- the radius of the cylinder R_{cyl} is an important parameter. If R_{cyl} is too large, two laterally displaced partial defects in opposite leaflets (one partial defect connected with the upper, one connected with the lower water compartment) may form, thereby filling all cylinder slices but not forming a continuous defect. In consequence, slight hysteresis between opening and closing pathways may appear. In previous work, we suggested $R_{\text{cyl}} = 1.2$ nm as suitable. However, we found that for very soft membranes, such as membranes of DLPG or DLPC, a smaller R_{cyl} is required to strictly avoid hysteresis. As such, we recommend a value of $R_{\text{cyl}} = 0.8$ nm or 1.0 nm for future work.

The chain coordinate has been implemented as an extension of GROMACS 2016 (Abraham, Murtola, Schulz, Páll, Smith, Hess, and Lindahl, 2015). The source code

of the implementation is available upon request from the authors of this chapter.

8. Summary and outlook

Pioneering simulations of pore formation used the collective radial and the flip-flop coordinate to induce pores. These simulations have provided unprecedented insight into mechanisms, atomic structures, and energetics involved in pore formation over lipid membranes. The simulations further revealed that a quantitative understanding of pores requires the calculation of free energies of pore formation.

In order to study the influence of factors such as lipid composition, electric fields, tension, or membrane-active agents on pore formation, it is critical to make sure that the PMFs are fully converged and that they do not suffer from hysteresis effects. Otherwise, given that the computed PMFs are modulated by such factors, it would remain unclear whether such factors influence (i) the magnitudes of hysteresis, or (ii) the true underlying free-energy surface. For example, the Lennard-Jones cutoff leads to different magnitudes of hysteresis with the flip-flop coordinate, but the underlying free-energy landscape is hardly influenced by the cutoff (Huang and García, 2014; Hub and Awasthi, 2017).

In addition, to understand how the lifetime of pores depends on external factors, it is necessary to detect the presence and the height of a free-energy barrier that may separate the open pore from the flat membrane, i.e. to detect whether the pore is metastable.

Therefore, we have presented an overview of four different reaction coordinates (RCs) that have been proposed for PMF calculations of pore formation using MD simulations: the radial collective coordinate, the flip-flop coordinate, the water density coordinate, and the chain coordinate. We found that the PMFs computed with umbrella sampling greatly depend on the choice of the RC. Specifically, we found that the radial collective RC may perturb the membrane more strongly than required for pore formation. In addition, the radial collective and the flip-flop coordinate may suffer from pronounced hysteresis between opening and closing pathways, suggesting that PMFs computed along these RCs converge slowly. The water density coordinate revealed greatly reduced hysteresis. However, none of the three coordinates reveal the nucleation barrier in a DMPC membrane, inconsistent with the metastability of the open pore in free simulations, suggesting that the barrier was integrated out. These problems recently prompted the development of the chain coordinate, which was designed to probe the formation and rupture of the continuous hydrogen bond network over the membrane. We found that PMF calculations with the chain coordinate converge rapidly, they do not suffer from hysteresis, and they do not integrate out the pore nucleation barrier (if a barrier is present).

These recent developments may be readily used to probe how electric fields, membrane-active peptides, lipid composition, membrane curvature, or other factors shape the free-energy landscape of pore formation, with implications on membrane fusion and fission, virus-host interactions, and biotechnological applications.

Funding

References

Abidor, I., Arakelyan, V., Chernomordik, L., Chizmadzhev, Y., Pastushenko, V., and Tarasevich, M., 1979. 246 - electric breakdown of bilayer lipid membranes i. the main experimental facts and their qualitative discussion, *Bioelectrochem. and Bioenerg.*, 6 (1), 37 – 52.

Abraham, M.J., Murtola, T., Schulz, R., Páll, S., Smith, J.C., Hess, B., and Lindahl, E., 2015. GROMACS: High performance molecular simulations through multi-level parallelism from laptops to supercomputers, *SoftwareX*, 1, 19–25.

Akinlaja, J. and Sachs, F., 1998. The breakdown of cell membranes by electrical and mechanical stress, *Biophys. J.*, 75 (1), 247–254.

Awasthi, N. and Hub, J.S., 2016. Simulations of pore formation in lipid membranes: Reaction coordinates, convergence, hysteresis, and finite-size effects, *J. Chem. Theory Comput.*, 12 (7), 3261–3269, pMID: 27254744.

Bechara, C. and Sagan, S., 2013. Cell-penetrating peptides: 20 years later, where do we stand?, *FEBS letters*, 587 (12), 1693–1702.

Bennett, W.D., Sapay, N., and Tieleman, D.P., 2014. Atomistic simulations of pore formation and closure in lipid bilayers, *Biophys. J.*, 106 (1), 210–219.

Bennett, W.D. and Tieleman, D.P., 2011. Water defect and pore formation in atomistic and coarse-grained lipid membranes: pushing the limits of coarse graining, *J. Chem. Theory Comput.*, 7 (9), 2981–2988.

Bennett, W.D. and Tieleman, D.P., 2014. The importance of membrane defects lessons from simulations, *Acc. Chem. Res.*, 47 (8), 2244–2251.

Berger, O., Edholm, O., and Jähnig, F., 1997. Molecular dynamics simulations of a fluid bilayer of dipalmitoylphosphatidylcholine at full hydration, constant pressure, and constant temperature., *Biophys. J.*, 72, 2002–2013.

Best, R.B. and Hummer, G., 2005. Reaction coordinates and rates from transition paths, *Proc. Natl. Acad. of Sci. USA*, 102 (19), 6732–6737.

Böckmann, R.A., De Groot, B.L., Kakorin, S., Neumann, E., and Grubmüller, H., 2008. Kinetics, statistics, and energetics of lipid membrane electroporation studied by molecular dynamics simulations, *Biophys. J.*, 95 (4), 1837–1850.

Bolhuis, P.G., Chandler, D., Dellago, C., and Geissler, P.L., 2002. Transition path sampling: Throwing ropes over rough mountain passes, in the dark, *Annu. Rev. Phys. Chem.*, 53 (1), 291–318.

Brochard-Wyart, F., de Gennes, P., and Sandre, O., 2000. Transient pores in stretched vesicles: role of leak-out, *Physica A: Statistical Mechanics and its Applications*, 278 (1), 32 – 51.

Brogden, K.A., 2005. Antimicrobial peptides: pore formers or metabolic inhibitors in bacteria?, *Nat. Rev. Microbiol.*, 3 (3), 238–250.

Fuhrmans, M., Marelli, G., Smirnova, Y.G., and Müller, M., 2015. Mechanics of membrane fusion/pore formation, *Chem. Phys. Lipids*, 185, 109–128.

Gurtovenko, A.A., Anwar, J., and Vattulainen, I., 2010. Defect-mediated trafficking across cell membranes: insights from in silico modeling, *Chem. Rev.*, 110 (10), 6077–6103.

Gurtovenko, A.A. and Vattulainen, I., 2005. Pore formation coupled to ion transport through lipid membranes as induced by transmembrane ionic charge imbalance: atomistic molecular dynamics study, *J. Am. Chem. Soc.*, 127 (50), 17570–17571.

Herce, H., Garcia, A., Litt, J., Kane, R., Martin, P., Enrique, N., Rebolledo, A., and Milesi, V., 2009. Arginine-rich peptides destabilize the plasma membrane, consistent with a pore formation translocation mechanism of cell-penetrating peptides, *Biophys. J.*, 97 (7), 1917–1925.

Hu, Y., Sinha, S.K., and Patel, S., 2015. Investigating hydrophilic pores in model lipid bilayers using molecular simulations: correlating bilayer properties with pore-formation thermodynamics, *Langmuir*, 31 (24), 6615–6631.

Huang, K. and García, A.E., 2014. Effects of truncating van der waals interactions in lipid bilayer simulations, *J. Chem. Phys.*, 141 (10), 09B605_1.

Hub, J.S. and Awasthi, N., 2017. Probing a continuous polar defect: A reaction coordinate for

pore formation in lipid membranes, *J. Chem. Theory Comput.*, 13 (5), 2352–2366, pMID: 28376619.

Jahn, R., Lang, T., and Südhof, T.C., 2003. Membrane fusion, *Cell*, 112 (4), 519–533.

Kägi, D., Ledermann, B., Bürki, K., Seiler, P., Odermatt, B., Olsen, K.J., Podack, E.R., Zinkernagel, R.M., and Hengartner, H., 1994. Cytotoxicity mediated by T cells and natural killer cells is greatly impaired in perforin-deficient mice, *Nature*, 369, 31–37.

Karatekin, E., Sandre, O., Guitouni, H., Borghi, N., Puech, P.H., and Brochard-Wyart, F., 2003. Cascades of transient pores in giant vesicles: line tension and transport, *Biophys. J.*, 84 (3), 1734–1749.

Kirsch, S.A. and Böckmann, R.A., 2016. Membrane pore formation in atomistic and coarse-grained simulations, *Biochimica et Biophysica Acta (BBA) - Biomembranes*, 1858 (10), 2266 – 2277, biosimulations of lipid membranes coupled to experiments.

LaRocca, T., Stivison, E., Mal-Sarkar, T., Hooven, T., Hod, E., Spitalnik, S., and Ratner, A., 2015. CD59 signaling and membrane pores drive Syk-dependent erythrocyte necroptosis, *Cell death & disease*, 6 (5), e1773.

Law, R.H., Lukoyanova, N., Voskoboinik, I., Caradoc-Davies, T.T., Baran, K., Dunstone, M.A., DAngelo, M.E., Orlova, E.V., Coulibaly, F., Verschoor, S., Browne, K.A., Ciccone, A., Kuiper, M.J., Bird, P.I., Trapani, J.A., Saibil, H.R., and Whisstock, J.C., 2010. The structural basis for membrane binding and pore formation by lymphocyte perforin, *Nature*, 468 (7322), 447–451.

Lenertz, L.Y., Gavala, M.L., Hill, L.M., and Bertics, P.J., 2009. Cell signaling via the P2X7 nucleotide receptor: linkage to ros production, gene transcription, and receptor trafficking, *Purinergic signalling*, 5 (2), 175–187.

Leontiadou, H., Mark, A.E., and Marrink, S.J., 2004. Molecular dynamics simulations of hydrophilic pores in lipid bilayers, *Biophys. J.*, 86 (4), 2156–2164.

Leontiadou, H., Mark, A.E., and Marrink, S.J., 2006. Antimicrobial peptides in action, *J. Am. Chem. Soc.*, 128 (37), 12156–12161.

Marrink, S., Jähnig, F., and Berendsen, H., 1996. Proton transport across transient single-file water pores in a lipid membrane studied by molecular dynamics simulations., *Biophys. J.*, 71 (2), 632.

Marrink, S.J., Lindahl, E., Edholm, O., and Mark, A.E., 2001. Simulation of the spontaneous aggregation of phospholipids into bilayers, *J. Am. Chem. Soc.*, 123, 8638–8639.

Melikov, K.C., Frolov, V.A., Shcherbakov, A., Samsonov, A.V., Chizmadzhev, Y.A., and Chernomordik, L.V., 2001. Voltage-induced nonconductive pre-pores and metastable single pores in unmodified planar lipid bilayer, *Biophys. J.*, 80 (4), 1829–1836.

Mirjalili, V. and Feig, M., 2015. Density-biased sampling: A robust computational method for studying pore formation in membranes, *J. Chem. Theory Comput.*, 11 (1), 343–350.

Moroz, J. and Nelson, P., 1997. Dynamically stabilized pores in bilayer membranes, *Biophys. J.*, 72 (5), 2211 – 2216.

Neale, C., Madill, C., Rauscher, S., and Pomès, R., 2013. Accelerating convergence in molecular dynamics simulations of solutes in lipid membranes by conducting a random walk along the bilayer normal, *J. Chem. Theory Comput.*, 9 (8), 3686–3703.

Neale, C. and Pomès, R., 2016. Sampling errors in free energy simulations of small molecules in lipid bilayers, *Biochim. Biophys. Acta – Biomembranes*, doi:10.1016/j.bbamem.2016.03.006.

Neumann, E., Schaefer-Ridder, M., Wang, Y., and Hofschneider, P., 1982. Gene transfer into mouse lyoma cells by electroporation in high electric fields., *EMBO J.*, 1 (7), 841–845.

Pastor, R. and MacKerell Jr, A., 2011. Development of the CHARMM force field for lipids, *J. Phys. Chem. Lett.*, 2 (13), 1526–1532.

Sakuma, Y. and Imai, M., 2015. From vesicles to protocells: The roles of amphiphilic molecules, *Life*, 5 (1), 651–675.

Sapay, N.W.F.D.B. and Tieleman, D.P., 2009. Thermodynamicsof flip-flop and desorption for a systematic series of phosphatidylcholine lipids, *Soft Matter*, 5, 3295–3302.

Sengupta, D., Leontiadou, H., Mark, A.E., and Marrink, S.J., 2008. Toroidal pores formed by antimicrobial peptides show significant disorder, *Biochim. Biophys. Acta – Biomembranes*,

1778 (10), 2308–2317.

Tarek, M., 2005. Membrane electroporation: a molecular dynamics simulation, *Biophys. J.*, 88 (6), 4045–4053.

Tekle, E., Astumian, R., Friauf, W., and Chock, P., 2001. Asymmetric pore distribution and loss of membrane lipid in electroporated DOPC vesicles, *Biophys. J.*, 81 (2), 960–968.

Tepper, H.L. and Voth, G.A., 2005. Protons may leak through pure lipid bilayers via a concerted mechanism, *Biophys. J.*, 88 (5), 3095–3108.

Tieleman, D.P., Leontiadou, H., Mark, A.E., and Marrink, S.J., 2003. Simulation of pore formation in lipid bilayers by mechanical stress and electric fields, *J. Am. Chem. Soc.*, 125 (21), 6382–6383.

Tieleman, D.P. and Marrink, S.J., 2006. Lipids out of equilibrium: Energetics of desorption and pore mediated flip-flop, *J. Amer. Chem. Soc.*, 128 (38), 12462–12467.

Ting, C.L., Awasthi, N., Müller, M., and Hub, J.S., 2018. Metastable prepores in tension-free lipid bilayers, *Phys. Rev. Lett.*, 120 (12), 18103.

Tolpekina, T., Den Otter, W., and Briels, W., 2004. Nucleation free energy of pore formation in an amphiphilic bilayer studied by molecular dynamics simulations, *J. Chem. Phys.*, 121, 12060–12066.

Torrie, G.M. and Valleau, J.P., 1974. Monte Carlo free energy estimates using non-Boltzmann sampling: Application to the sub-critical Lennard-Jones fluid, *Chem. Phys. Lett.*, 28, 578–581.

Vorobyov, I., Olson, T.E., Kim, J.H., Koeppe, R.E., Andersen, O.S., and Allen, T.W., 2014. Ion-induced defect permeation of lipid membranes, *Biophys. J.*, 106 (3), 586–597.

Wimley, W.C., 2010. Describing the mechanism of antimicrobial peptide action with the interfacial activity model, *ACS Chem. Biol.*, 5 (10), 905–917.

Wohlert, J., den Otter, W.K., Edholm, O., and Briels, W.J., 2006. Free energy of a trans-membrane pore calculated from atomistic molecular dynamics simulations, *J. Chem. Phys.*, 124 (15), 154905.

Zasloff, M., 2002. Antimicrobial peptides of multicellular organisms, *Nature*, 415 (6870), 389–395.

Zhelev, D.V. and Needham, D., 1993. Tension-stabilized pores in giant vesicles: determination of pore size and pore line tension, *Biochim. Biophys. Acta – Biomembranes*, 1147 (1), 89–104.